© 2014. Published by The Company of Biologists Ltd | Development (2014) 141, 158-165 doi:10.1242/dev.097568

RESEARCH ARTICLE

Retinoic acid controls proper head-to-trunk linkage in zebrafish by regulating an anteroposterior somitogenetic rate difference

Bambang Retnoaji[1,2], Ryutaro Akiyama[1,3], Tatsuro Matta[1], Yasumasa Bessho[1] and Takaaki Matsui[1,*]

ABSTRACT

During vertebrate development, the primary body axis elongates towards the posterior and is periodically divided into somites, which give rise to the vertebrae, skeletal muscles and dermis. Somites form periodically from anterior to posterior, and the anterior somites form in a more rapid cycle than the posterior somites. However, how this anteroposterior (AP) difference in somitogenesis is generated and how it contributes to the vertebrate body plan remain unclear. Here, we show that the AP difference in zebrafish somitogenesis originates from a variable overlapping segmentation period between one somite and the next. The AP difference is attributable to spatiotemporal inhibition of the clock gene *her1* via retinoic acid (RA) regulation of the transcriptional repressor *ripply1*. RA depletion thus disrupts timely somite formation at the transition, eventually leading to the loss of one somite and the resultant cervical vertebra. Overall, our results indicate that RA regulation of the AP difference is crucial for proper linkage between the head and trunk in the vertebrate body plan.

KEY WORDS: Somitogenesis, Axis elongation, Live imaging, Zebrafish

INTRODUCTION

During vertebrate development, the period of somite segmentation depends on a segmentation clock that is controlled by cyclically expressed genes such as Notch effectors, whereas the position of segmentation is determined by opposed gradients of fibroblast growth factor (FGF) and retinoic acid (RA) (Dubrulle et al., 2001; Holley, 2007; Pourquié, 2001; Sawada et al., 2001). Anterior somites, which give rise to part of the skull and the cervical vertebrae, are formed early, and posterior somites, from which the thoracic, lumbar and sacral vertebrae originate, then arise progressively as the axis elongates (Holley, 2006; Holley, 2007; Morin-Kensicki et al., 2002). Although it might be expected that, to generate the perfectly repetitive pattern of both somites and the resultant vertebrae, the periodicity of somite segmentation should be constant throughout somitogenesis, a substantial difference between anterior and posterior somitogenesis has been observed in several species, including amphioxus, mouse and zebrafish (Hanneman and Westerfield, 1989; Kimmel et al., 1995; Schubert et al., 2001; Tam, 1981). In zebrafish, for instance, the anterior somites form every 20 minutes, whereas the posterior somites form every 30 minutes (Hanneman and Westerfield, 1989; Kimmel et al., 1995). However, how the pace of somitogenesis changes and how this anteroposterior (AP) difference contributes to the later body plan remain unclear.

In this study, we observed somite segmentation in zebrafish embryos and showed that the AP difference is generated by a variable overlap in segmentation period for successive somites. We also found that a rate transition from anterior to posterior somitogenesis is regulated by RA signaling and is required for controlling somite/vertebra number and for correct linkage of the head to the trunk. Our results therefore answer crucial and longstanding questions about the formation of vertebrate segments.

RESULTS

A variable overlap in segmentation period for successive somites causes a difference between anterior and posterior somitogenesis

To investigate what happens during the AP transition, we monitored the formation of the first eight somites by time-lapse imaging and found a difference between the first four and the later four somites: the first four, which are the anterior somites, formed quickly, whereas the posterior somites 5 to 8 formed more slowly (supplementary material Fig. S4 and Movie 1A,B). More posterior somites (for example, somites 9 to 12) also formed at a rate similar to that of somites 5 to 8 (supplementary material Movie 2). These observations confirmed that there is a rate/pace difference between anterior and posterior somitogenesis in zebrafish.

As the period of morphological somite formation is the same for the trunk somites (somites 6 to 18) (Schröter et al., 2008), we reasoned that the AP difference is generated by a distinction of segmentation between anterior and posterior somites. To test this possibility, we determined precisely when segmentation begins and ends (for details, see supplementary material Fig. S1 and Materials and methods), and estimated the segmentation period for each somite (Fig. 1A). Unexpectedly, we could not detect any statistically significant difference in segmentation period between somites 1 and 8 (28.9±2.1 minutes; Fig. 1B; supplementary material Table S1). Instead, we found a significant difference ($P<0.05$) between somites 1-4 and somites 5-8 in the interval between the segmentation start of one somite and the start of the next somite (termed ‘start to start’; Fig. 1C; supplementary material Table S3). Particularly for somites 1 to 4, because the next furrow was visible before the current boundary has completely formed, segmentation periods of anterior somites 1-4 highly overlapped by 13.6±2.5 minutes (47% of the segmentation period). By contrast, the overlap time for posterior somites 5 to 8 was only 2.7±2.5 minutes (9% of the segmentation period) (Fig. 1A-E). This difference between anterior and posterior somitogenesis was also seen in other zebrafish strains (Riken-wako, India and TL) (supplementary material Fig. S5A-C), indicating that the AP difference is not strain specific. These results therefore suggest that the AP difference is generated by variation in the overlap of segmentation period between one somite and the next somite.

[1]Gene Regulation Research, Graduate School of Biological Sciences, Nara Institute of Science and Technology, 8916-5 Takayama, Nara 630-0101, Japan. [2]Faculty of Biology, Gadjah Mada University, Jl. Teknika Selatan, Sekip Utara, Bulaksumur, Yogyakarta 55281, Indonesia. [3]Department of Genetics, Cell Biology and Development, University of Minnesota, 321 Church Street SE, 6-160 Jackson Hall, Minneapolis, MN 55455, USA.

*Author for correspondence (matsui@bs.naist.jp)

Received 15 April 2013; Accepted 8 October 2013

Development (2014) doi:10.1242/dev.097568

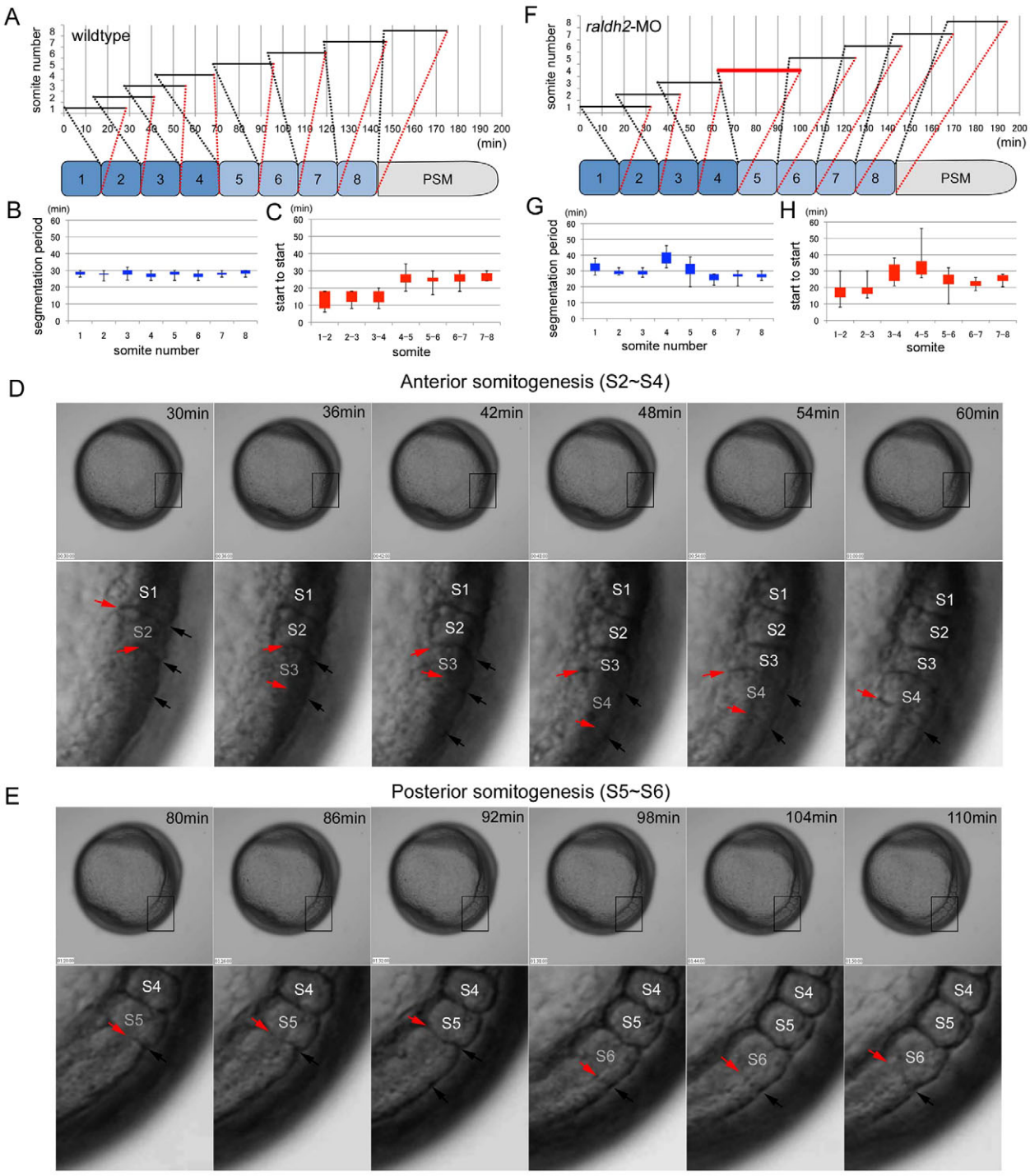

Fig. 1. Knockdown of *raldh2* results in a failure of AP transition. (A) Time-lapse data for somitogenesis in a wild-type zebrafish embryo (supplementary material Movie 1A,B). Black bars indicate periods between segmentation start and end. Successive segmentations overlap in somites 1-4. (B) Segmentation periods in wild-type embryos are constant. Segmentation periods (black bars in A) are extracted from wild-type embryos (*n*=9) and shown as box and whisker plots (minimum, 25% percentile, 75% percentile, and maximum). (C) Overlapping rates of segmentations differ between anterior somites 1-4 and posterior somites 5-8. Box and whisker plots of 'start to start', the interval between segmentation starts for one somite and the next, in wild-type embryos (*n*=9). (D) Typical images for anterior somitogenesis. Time-lapse images from 30 minutes to 60 minutes (6-minute intervals) in the wild-type zebrafish embryo (A) are displayed. Lower panel: higher-magnification views of boxed areas. Black arrows indicate the dorsal limit of the furrow of forming somite. Red arrows indicate the ventral limit of the furrow. Segmentations overlap in somites 2-4 (S2-S4). (E) Typical images for posterior somitogenesis. Time-lapse images from 80 minutes to 110 minutes (6-minute intervals) in the wild-type zebrafish embryo (A) are displayed. Lower panel: higher-magnification views of boxed areas. Black arrows indicate the dorsal limit of the furrow of newly formed somite. Red arrows indicate the ventral limit of the furrow. Segmentations in somites 5 and 6 (S5 and S6) occur sequentially. (F) Time-lapse data for somitogenesis in a *raldh2* MO-injected embryo (supplementary material Movie 3A,B). The segmentation period of somite 4 (red bar) was longer than that of the wild-type embryo (A). (G,H) Box and whisker plots of segmentation period (G) or start to start (H) for *raldh2* MO-injected embryos (*n*=10). *raldh2* knockdown results in a prolonged segmentation period for somite 4 and the failure of proper AP transition. Results from statistical analyses are shown in supplementary material Tables S1-S4.

Development (2014) doi:10.1242/dev.097568

RA signaling regulates the crucial segmentation period of somite 4, ensuring the normal AP transition

Vertebrate somite segmentation is regulated by Notch, FGF and RA activities (Dubrulle et al., 2001; Holley, 2007; Pourquié, 2001; Sawada et al., 2001). To test whether these signals control the AP transition, we inhibited their activity using antisense morpholino oligonucleotides (MOs). Although knockdown of the Notch ligand *deltad* or the FGF ligand *fgf8a*, which is known to disrupt Notch or FGF signaling in the context of somitogenesis (Draper et al., 2003; Dubrulle et al., 2001; Duester, 2007; Mara et al., 2007; Wright et al., 2011), had no effect on the AP transition (supplementary material Fig. S5D,E), knockdown of *raldh2* (*aldh1a2* – Zebrafish Information Network) a major source of RA in the context of somitogenesis (Begemann et al., 2001; Duester, 2007), was detrimental. *raldh2* morphants displayed an extension of the segmentation period at somite 4, leading to failure of the AP transition (Fig. 1F-H; supplementary material Tables S1, S2 and Movie 3A,B).

Time-lapse imaging of somitogenesis revealed that 8 and 7 somites were formed within 180 minutes in wild-type embryos and *raldh2* morphants, respectively (Fig. 1A,F; supplementary material Movies 1, 3). These results suggest that failure of the AP transition affects the total number of somites. We therefore counted somite number in *raldh2* morphants at later stages. *raldh2* morphants displayed a persistent one-somite deficiency relative to control embryos throughout 12-16 hours post fertilization (hpf) (Fig. 2A,B; supplementary material Table S6), suggesting that a proper AP transition is required to control the number of somites.

The AP transition is required for correct linkage of the head to the trunk

Because a vertebra is formed from the caudal part of one somite and the rostral part of the next somite, somite and vertebra numbers are correlated (Morin-Kensicki et al., 2002). The first two somites do not contribute to the zebrafish vertebral column, whereas somites 3 to 34 give rise to 32 vertebrae: two cervical, ten rib-bearing, two rib- and hemal-arch-bearing, 14 hemal-arch-bearing and four tail fin set vertebrae are formed from anterior to posterior (Morin-Kensicki et al., 2002). As *raldh2* morphants lose a somite owing to failure of the AP transition, it seems possible that *raldh2* morphants should subsequently display a missing vertebra. Alternatively, as RA treatment is known to change vertebral subtypes through the regulation of Hox genes (Geelen, 1979; Kessel and Gruss, 1991), it is also possible that *raldh2* knockdown may induce homeotic transformation. To test whether *raldh2* knockdown leads to loss of vertebrae, change of vertebral subtypes or both, we enumerated the number of vertebrae in *raldh2* morphants by staining the bones and cartilage. Although bones and cartilage within the vertebral column of *raldh2* morphants looked normal, *raldh2* knockdown resulted in loss of a specific vertebra, the second cervical vertebra (Fig. 2C,D; supplementary material Table S8). This phenotype was not likely to be induced by homeotic transformation. Rather, because the second cervical vertebra is derived from both the caudal part of somite 4 and the rostral part of somite 5, loss of the second cervical vertebra in *raldh2* morphants is consistent with the earlier defect in the AP transition occurring during the segmentation of somite 4 (Fig. 1F-H). These results suggest that RA depletion fails to ensure the segmentation period of somite 4 and the AP transition, leading to the loss of a somite and eventually of the resultant neck vertebra. Our results therefore uncover a novel mechanism, in which RA controls proper head-to-trunk linkage in zebrafish by regulating the segmentation period of somite 4 and the AP transition.

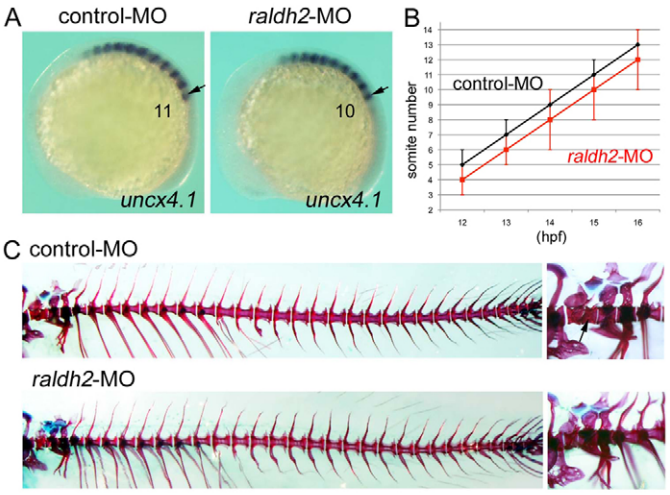

D control-MO

Vertebrae	Averages±s.d.	Minimum	Maximum	Mode	n
Total	32.2±0.9	31	34	32	18
Cervical	2.0±0.0	2	2	2	18
Rib Bearing	10.2±0.4	10	11	10	18
Rib and hemal arch bearing	1.9±0.3	1	2	2	18
Hemal arch bearing	15.1±0.8	14	16	15	18
Tail fin set	3.0±0.0	3	3	3	18

raldh2-MO

Vertebrae	Averages±s.d.	Minimum	Maximum	Mode	n
Total	31.2±1.1	29	33	31	17
Cervical	1.3±0.5	1	2	1	17
Rib Bearing	9.9±0.3	9	10	10	17
Rib and hemal arch bearing	1.9±0.3	1	2	2	17
Hemal arch bearing	15.2±0.9	14	17	15	17
Tail fin set	2.9±0.4	2	4	3	17

Fig. 2. Knockdown of *raldh2* leads to loss of a somite and the resultant second cervical vertebra. (A) Representative images of *uncx4.1* expression in control MO- (left) or *raldh2* MO-injected (right) embryos at 15 hpf. Lateral view, anterior to the left. Arrows mark the position at SI. (B) Somite numbers in control MO- (black; *n*=32, 45, 47, 47 and 48) or *raldh2* MO-injected (red; *n*=34, 38, 55, 55 and 56) embryos at 12, 13, 14, 15 and 16 hpf. Error bars indicate s.d. *raldh2* morphants lack one somite. (C) Representative images of skeletal structures in control MO-(upper panel) or *raldh2* MO-injected (lower panel) fish at 1.5 months old. Bones (red) and cartilage (blue) are stained by Alizarin Red and Alcian Blue, respectively. Right: higher-magnification views of the cervical vertebrae (right panels). The second cervical bone (arrow in upper right image) forms in control MO-injected fish, but is missing in *raldh2* MO-injected embryos (lower right). (D) Vertebra number in control MO- or *raldh2* MO-injected fish. Results from statistical analyses are shown in supplementary material Tables S5, S6, S8.

RA supply during late gastrulation is sufficient for controlling the AP transition

Although segmentation of somite 4 occurs during 11-12 hpf (somitogenesis stages), the future somite boundary of this somite is determined earlier, during 9-10 hpf (gastrulation stages). Thus, we do not yet know whether a supply of RA during gastrulation, somitogenesis or both is required for a proper AP transition. To address this question, we treated embryos with diethylaminobenzaldehyde (DEAB), an RA synthesis enzyme inhibitor (Grandel and Brand, 2011; Hamade et al., 2006), in embryos during different time windows. DEAB treatment during 4-10 hpf (gastrulation stages), but not 10-14 hpf (somitogenesis stages), led to the loss of one somite (supplementary material Fig. S6A,B) and the failure of the AP transition (supplementary material Fig. S6C-E, Tables S1-S4 and Movie 4A,B), phenotypes

Development (2014) doi:10.1242/dev.097568

that were reminiscent of *raldh2* morphants (Fig. 2A,B; supplementary material Table S6). Importantly, transient RA administration in *raldh2* morphants during 4-10 hpf could partially restore the loss of somite (Fig. 3A; supplementary material Table S7) and vertebra phenotypes (Fig. 3B). These results suggest that RA supply during gastrulation plays a crucial role in controlling somite number by adjusting the segmentation period of somite 4. To test this possibility, we performed time-lapse analyses for *raldh2* morphants treated with RA during 4-10 hpf. As expected, RA could rescue the segmentation period of somite 4 and the AP transition in *raldh2* morphants (Fig. 3C-E; supplementary material Tables S1-S4 and Movie 5A,B). More specifically, RA treatment during 7-10 hpf could also rescue the defect of the AP transition in *raldh2* morphants (data not shown). These results therefore indicate that RA supply before somite segmentation stages (during gastrulation) is important for controlling the AP transition, which is a prerequisite step for determining the number of somites and resultant vertebrae.

The AP transition is facilitated by RA/Ripply1-mediated spatiotemporal regulation of the *her1* segmentation clock

We next investigated how RA controls the AP transition during gastrulation. As RA is implicated in the determination of somite size by antagonizing an opposed FGF gradient during somitogenesis (Duester, 2007), we tested the expression of *fgf8a*, *mespb* (*mespba* – Zebrafish Information Network) and *papc* (*pcdh8* – Zebrafish Information Network), which is controlled by the RA/FGF gradient (Fior et al., 2012; Hamade et al., 2006; Holley, 2007; Kawakami et al., 2005; Lee et al., 2009; Yamamoto et al., 1998). However, we could not find a clear difference in expression between control and *raldh2* morphants (supplementary material Fig. S7), suggesting that RA-dependent inhibition of FGF signaling is unlikely to regulate the AP transition. This is also supported by the observation that the AP transition occurred normally in *fgf8a* morphants (supplementary material Fig. S5E).

As RA depletion transiently affects the tempo of somite segmentation (Resende et al., 2010), another possibility is that RA spatially and temporally regulates the segmentation clock during the AP transition. To determine whether such a mechanism exists, we investigated the integrity of the somite segmentation clock in *raldh2* morphants during late gastrulation by monitoring the expression of the cyclic gene *her1*, a major component of the zebrafish segmentation clock (Gajewski et al., 2003; Henry et al., 2002). *raldh2* morphants at 9 hpf showed a wave-like propagation of *her1* expression in a manner similar to control embryos, although the width of the *her1* stripes was larger (Fig. 4A). The number of *her1* stripes in control embryos increased from two to three by 10 hpf, whereas only two stripes could be seen in *raldh2* morphants at 10 hpf owing to the absence of the most anterior *her1* stripe ($P<0.05$; Fig. 4A). As the number of *her1* stripes in *raldh2* morphants increased to three by 11 hpf (Fig. 4A), the increase of *her1* stripe number was therefore delayed in *raldh2* morphants at late gastrulation. Proper transition between anterior and posterior somitogenesis may thus require an increase of *her1* stripe number within the paraxial mesoderm at the time when the future boundary of somite 4 is determined, of which RA signaling may control this process.

When we compared *her1* expression between control and *raldh2* morphants at 10 hpf, we noticed that the upper stripes of *her1* were thinner than those of control morphants (Fig. 4A), suggesting that RA signaling suppresses *her1* expression at the anterior part of the paraxial mesoderm at late gastrulation through an unidentified effector(s). Ripply1 is known to repress the transcription of specific genes, which are targets of T-box transcription factor family members, by recruiting the co-repressor Groucho (Kawamura et al., 2005). As *ripply1* knockdown results in the expansion of *her1* expression into somite regions during somitogenesis, and as *her1* expression is controlled by the three T-box family members *spadetail* (*tbx16* – Zebrafish Information Network), *no tail*, *fused*

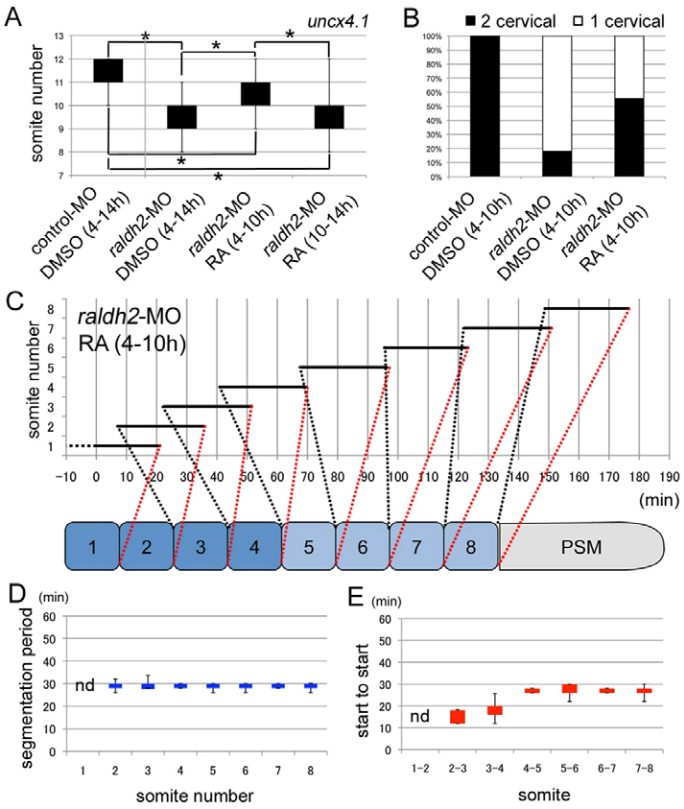

Fig. 3. RA administration during gastrulation partially restores the failure of AP transition. (A) Box and whisker plots of somite number in control MO-injected embryos treated with dimethyl sulfoxide (DMSO) (vehicle) during 4-14 hpf (n=37) or *raldh2* MO-injected embryos treated with either DMSO during 4-14 hpf (n=48), RA during 4-10 hpf (n=39) or RA during 10-14 hpf (n=44). Asterisks indicate statistically significant differences ($P<0.05$; see also supplementary material Table S7). (B) Number of second cervical vertebrae. Black and white bars indicate two and one cervical vertebrae, respectively. All control MO-injected fish treated with DMSO during 4-10 hpf have two cervical vertebrae (n=18). More than 80% of *raldh2* morphants treated with DMSO during 4-10 hpf (n=28) have only one cervical vertebra because the second cervical vertebra is lost, whereas 55% of *raldh2* morphants treated with RA during 4-10 hpf have two cervical vertebrae (n=31), suggesting that RA treatment during gastrulation partially restores the loss-of-vertebra phenotype in *raldh2* morphants. Statistically significant differences ($P<0.05$) could be seen in control MO + DMSO versus *raldh2* MO + DMSO ($P=0.24\times10^{-7}$), control MO + DMSO versus *raldh2* MO + RA ($P=0.62\times10^{-2}$), and *raldh2* MO + DMSO versus *raldh2* MO + RA ($P=0.62\times10^{-3}$). (C) Time-lapse data of somitogenesis in a *raldh2* MO-injected embryo treated with RA during 4-10 hpf. After *raldh2* MO-injected embryos had been treated with RA during 4-10 hpf, embryos were mounted in low melting agarose and somitogenesis was observed at 2-minute intervals for 180 minutes. Because segmentation of somite 1 had already begun at the start of time-lapse, we could not determine the segmentation period for somite 1 or the start to start duration for somites 1-2. (D,E) Box and whisker plots of segmentation period (D) and start to start (E) of *raldh2* MO-injected embryos treated with RA during 4-10 hpf (n=5). Treatment of *raldh2* morphants with RA during 4-10 hpf rescues the failures of the segmentation period of somite 4 and the AP transition. Additional data from statistical analyses are shown in supplementary material Tables S1-S4. nd, not determined.

Development (2014) doi:10.1242/dev.097568

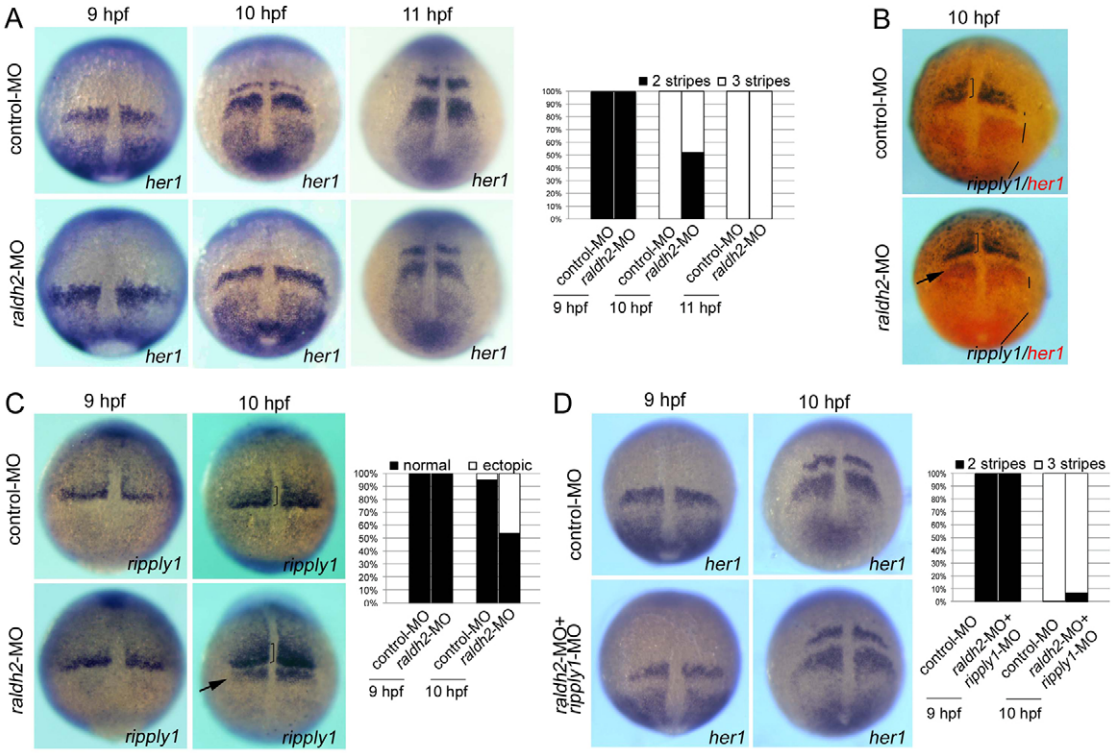

Fig. 4. Relationship between *her1* and *ripply1* expression during gastrulation. (A) Representative images of *her1* expression in control MO- (upper panel; *n*=33, 37 and 26) and *raldh2* MO-injected embryos at 9, 10 and 11 hpf (lower panel; *n*=35, 29 and 21). Dorsal view, anterior to the top. The increase in stripe number for *her1* expression in control embryos is delayed in *raldh2* morphants (right graph). A statistically significant difference could be seen between embryos injected with control MO and *raldh2* MO ($P<0.05$, $P=0.29\times10^{-6}$). (B) Double staining of *her1* (red) and *ripply1* (purple) in control MO- (upper panel) and *raldh2* MO-injected (lower panel) embryos at 10 hpf. (C) Representative images of *ripply1* expression in control MO- (upper panel) and *raldh2* MO-injected (lower panel) embryos at 9 and 10 hpf. Ectopic expression of *ripply1* could be observed in *raldh2* morphants at 10 hpf (arrow) ($P<0.05$, $P=0.50\times10^{-7}$; right graph). (D) Representative images of *her1* expression in control MO- (upper panel; *n*=58 and 52) and *raldh2* MO + *ripply1* MO-injected (lower panel; *n*=63, and 59) embryos at 9, 10 and 11 hpf. Dorsal view, anterior to the top. Decreased number of the *her1* stripe in *raldh2* morphants could be restored by co-injection of *ripply1* MO (right graph). A statistically significant difference was observed in embryos (10 hpf) injected with *raldh2* MO versus embryos (10 hpf) injected with *raldh2* MO + *ripply1* MO ($P<0.05$, $P=0.42\times10^{-5}$), but not in embryos (10 hpf) injected with control MO versus embryos (10 hpf) injected with *raldh2*- MO + *ripply1* MO ($P>0.05$, $P=0.12$).

somites (*tbx6* – Zebrafish Information Network) (Garnett et al., 2009; Holley et al., 2000; Nikaido et al., 2002), it seemed possible that, by mediating RA signaling, Ripply1 suppresses *her1* expression during the AP transition.

To test whether RA signaling affects *ripply1* expression during late gastrulation, we investigated *ripply1* expression in *raldh2* morphants and found that an extra stripe of *ripply1* could be seen at a location close to where the anterior stripe of *her1* was lost (Fig. 4C). Importantly, two-color *in situ* hybridization of *her1* and *ripply1* revealed that the extra stripe of *ripply1* was adjacent to the second stripe of *her1* in *raldh2* morphants (Fig. 4B). If this is the case, double knockdown of *raldh2* and *ripply1* should be able to rescue the effect of *raldh2* knockdown for the number of *her1* stripes. To test this possibility, we co-injected *raldh2* MO and *ripply1* MO and found a significant rescue phenotype for the number of *her1* stripe ($P<0.05$; Fig. 4A,D). Therefore, our results suggest a possibility that the failure of AP transition is caused by RA/Ripply1-mediated spatial and temporal inhibition of *her1* expression.

To investigate this further, we overexpressed either Ripply1 or Ripply1ΔWRPW, which cannot interact with Groucho (Kawamura et al., 2005), and performed *in situ* hybridization of *her1* in the manipulated embryos. Although overexpression of Ripply1ΔWRPW did not affect *her1* expression in the presomitic mesoderm (PSM) at 12 hpf, overexpression of Ripply1 inhibited *her1* expression (Fig. 5A). Taken together, our results suggest that RA/Ripply1-mediated spatial and temporal regulation of *her1* propagation leads to a proper transition from anterior to posterior somitogenesis (Fig. 5B).

DISCUSSION

RA signaling plays crucial roles in multiple developmental processes. In the case of somitogenesis, it has been reported that either complete loss of *raldh2* (a major source of RA during development) or treatment of excess RA results in defects in the expression of Hox genes, differentiation of somite cells, wavefront formation and symmetric somite formation (Begemann et al., 2001; Geelen, 1979; Holley, 2007; Kawakami et al., 2005; Kessel and Gruss, 1991; Niederreither and Dollé, 2008). However, a defect in AP transition in manipulated embryos has not been observed. In the present study, we partially knocked *raldh2* down in zebrafish embryos and showed a novel requirement of RA signaling for the AP transition.

Why does partial knockdown of *raldh2* lead to the specific defect in AP transition? This may be explained by the differences in sensitivity towards RA between the processes of somitogenesis. In embryos injected with 1.7 ng *raldh2* MO (partial knockdown situation), in which RA signaling is weakly activated

Development (2014) doi:10.1242/dev.097568

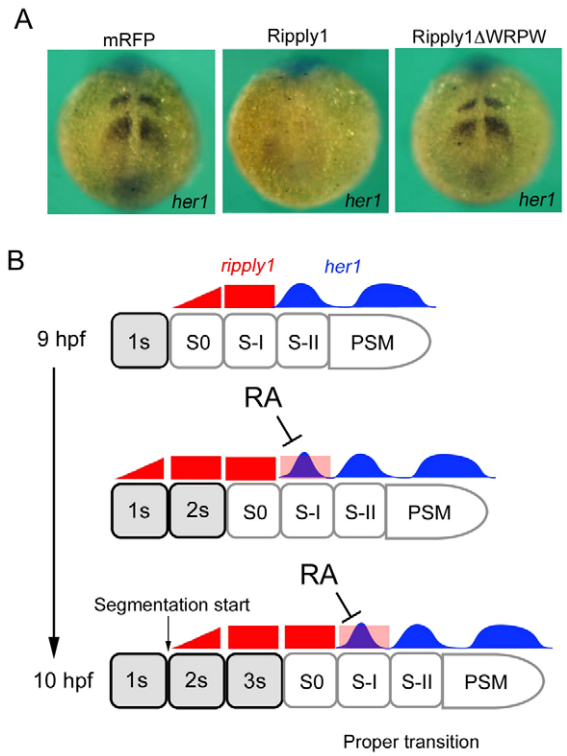

Fig. 5. Proposed mechanism for the proper transition from anterior to posterior somitogenesis. (A) *her1* expression in embryos at 12 hpf overexpressing mRFP (*n*=40), Ripply1 (*n*=32) or Ripply1ΔWRPW (*n*=38). Overexpression of Ripply1, but not Ripply1ΔWRPW, inhibited *her1* expression in the PSM at 12 hpf. (B) Proper transition between anterior and posterior somitogenesis. RA inhibits *ripply1* expression at the S-I position, leading to a proper increase in the number of *her1* stripes by 10 hpf. This allows the transition of anterior and posterior somitogenesis to occur normally. This regulation is required to control somite number and proper linkage between head and trunk during zebrafish development.

(supplementary material Fig. S2), a small amount of RA generated by the rest of *raldh2* and/or other sources of RA is not sufficient to regulate the AP transition, but sufficient for controlling other processes of somitogenesis (Fig. 1F-H; Fig. 2C,D).

A future somite boundary is determined at a position where *her1* segmentation clock meets wavefront generated by FGF/RA gradients (Holley, 2007; Pourquié, 2001). Based on the positional information, *mespb* starts to express at the right position (rostral side of S-II), and then morphological somite segmentation takes place at B-1 (the boundary between S0 and S-I) (Holley, 2007; Pourquié, 2001). Because many processes such as gene expression, signal transduction and differentiation of PSM cells occur during a duration from the establishment of the future somite boundary to morphological segmentation of the resultant somite, it is easy to imagine that the duration is not short.

We realized that morphological segmentation between somite 4 and 5 occurring at around 11-12 hpf was delayed in *raldh2* morphants (Fig. 1A,F). We also found a delay in the increase in *her1* stripe during 10-11 hpf (Fig. 4A). Our results suggest a possibility that, in *raldh2* morphants, the delay of morphological segmentation between somite 4 and 5 is caused by the delay in the increase of *her1* stripe during late gastrulation. In other words, although the future boundary between somite 4 and 5 is established at the time (during 9-10 hpf) when the anteriormost *her1* stripe appears and in the position (within the elongating paraxial mesoderm) where the anteriormost *her1* stripe meets wavefront in wild-type embryos, only the timing of the formation of the future somite boundary is affected in *raldh2* morphants. This possibility is supported by the data showing that the repetitive structures of somites looked normal in *raldh2* morphants (supplementary material Movie 3A,B) and that the timing of morphological segmentation between somite 4 and 5 could be restored in *raldh2* morphants treated with RA (4-10 or 7-10 hpf) (Fig. 3C-E; supplementary material Movie 5, 5-1).

During epiboly/gastrulation, the paraxial mesoderm regions including somite progenitor cells elongate quickly. During 90-100% epiboly (9-10 hpf), the number of *her1* stripe increases from two to three within the elongating paraxial mesoderm in control embryos (Fig. 4A; Fig. 5B). However, the third strip of *her1* did not appear by 10 hpf in *raldh2* morphants although epiboly occurred normally (Fig. 4A). Thus, it seemed that an integration of clock and wavefront takes place in a different manner: The integration occurs at a position adjacent to the second and third stripe of *her1* at 9 and 10 hpf, respectively. Our results therefore suggest that smooth increase of *her1* stripe during 9-10 hpf is required for the proper transition of anterior- to posterior-somitogenesis, and that RA signaling represses *ripply1* expression at an anterior region of the second stripe of *her1*, and regulates timing of the appearance of the third stripe of *her1* to achieve the proper AP transition.

In *raldh2* morphants, the period of morphological segmentation of somite 4 became longer (Fig. 1F,G). As RA is known to control the tempo of segmentation clock in chick (Resende et al., 2010), it is possible that RA signaling affects the period of *her1* oscillation. However, this is not likely because the timing for morphological segmentation of somite 4 is different from that of the future somite boundary formation, which occurred at around 10 hpf. Although it is expected that either the activity of somite segmentation machineries (such as Ephs and Ephrins) (Holley, 2007) or cellular responses (or both) is altered in *raldh2* morphants, how partial knockdown of *raldh2* affects segmentation period of somite 4 remains unclear. Because these processes are dynamic, it would be of great interest to observe spatial and temporal dynamics of segmentation clock and wavefront coupled with morphological segmentation.

Conclusions

The difference between anterior and posterior somitogenesis was first observed in zebrafish about 30 years ago. However, how the AP difference occurs during development has remained unknown. In this study, we provide the first evidence that the AP difference is explained by variation in the duration of an overlap between successive somite segmentation periods. We also provide insight into the molecular mechanism by which transient repression of propagation of the *her1* clock controls the proper transition from shorter to longer somitogenetic periodicity. Furthermore, our results reveal that the proper AP transition of somitogenesis is a prerequisite step for the correct linkage of head and trunk in the vertebrate body plan.

MATERIALS AND METHODS

Zebrafish and whole-mount *in situ* hybridization

Wild-type zebrafish and zebrafish wild-type strains (Riken-wako, India and TL) were used in this study. Single- or double-color whole-mount *in situ* hybridization was performed as described previously (Matsui et al., 2005; Matsui et al., 2011). cDNA fragments of *fgf8a*, *her1*, *mespb*, *papc*, *ripply1*,

tbx24 (*tbx6* – Zebrafish Information Network), *uncx4.1* and *Venus* were used as templates for antisense probes.

Time-lapse imaging and measurement of somitogenesis period

Embryos at 6-7 hpf were manually dechorionated and embedded in 1% low melting agarose. Time-lapse image acquisition was performed with an Olympus FV-1000-D confocal microscope and FLUOVIEW software. *Z*-stack images (ten planes and 17.15-µm intervals) were obtained every 2 minutes at 28.5°C. Using Metamorph software, images were combined into a time-stack, time-stamped and saved as a TIFF-stack and MOV movie.

From each somitogenesis movie, the time of segmentation start and end was visually annotated. Because somite boundary formation starts from the dorsal side in the lateral view, the start of segmentation (0 minutes) was defined as when a furrow appeared at the dorsal limit of the PSM (supplementary material Fig. S1A). Segmentation was considered to have ended when the boundary was clearly visible and the somite was completely separated from the PSM (supplementary material Fig. S1B).

Skeletal staining

Fish (1.5 months old) were fixed with 99.9% ethanol for at least 24 hours and their scales and internal organs were removed. They were treated with acetone for 24 hours, and then incubated in staining solution (0.015% Alcian Blue, 0.015% Alizarin Red in 70% ethanol) at 37°C for 2-3 days. After being washed with water, the fish were cleared using 1% potassium hydroxide (KOH) for 12-24 hours, and successively incubated in 1% KOH in 20% glycerol and 0.01% KOH in 20% glycerol. Stained fish were stored in 50% glycerol.

DEAB treatment

Embryos were treated with 10 µM DEAB (Tokyo Kasei) during either 4-10 or 10-14 hpf, and washed extensively with fish water. Embryos were then fixed and used for *in situ* hybridization.

Morpholinos, mRNA and injection

The following antisense MO oligonucleotides against *raldh2*, *deltad* (*deltaD* – Zebrafish Information Network), *fgf8a* and a control MO were obtained from Gene Tools: control MO: 5′-CCTCTTACCTCAGTTACAATTTATA-3′; *deltad* MO: 5′-AACAGCTATCATTAGTCGTCCCATG-3′ (Kawamura et al., 2008) (a gift from Dr Shinji Takada); *fgf8a* MO: 5′-GAGTCTCATGTTTATAGCCTCAGTA-3′ (Matsui et al., 2011); *raldh2* MO: 5′-GTTCAACTTCACTGGAGGTCATC-3′ (Begemann et al., 2001; Kawakami et al., 2005).

The plasmids pCS2-*ripply1*, pCS2-*ripply1ΔWRPW* (gifts from Dr Shinji Takada) and pCS2-*monomeric red fluorescent protein* (*mRFP*) were used in this study. *ripply1*, *ripply1ΔWRPW* and *mRFP* mRNA were synthesized using the SP6 mMessage mMachine System (Ambion).

For *in situ* hybridization and skeletal staining, *raldh2* MO (1.7 ng) or control MO (1.7 ng) were injected into the yolk of one-cell-stage zebrafish embryos. Embryos were fixed at the indicated time points.

neckless (*nls*; *aldh1a2* – Zebrafish Information Network) mutants display a variety of developmental defects, such as small hindbrain, lack of pectoral fins, asymmetric somite formation, small somites and short body (Begemann et al., 2001; Kawakami et al., 2005). However, injection of 1.7 ng *raldh2* MO led to milder phenotypes compared with those of *nls* mutants (supplementary material Fig. S3). To test whether this amount of *raldh2* MO could inhibit RA signaling in zebrafish embryos, we generated a transgenic line *Tg[RARE:Venus]* by using Tol2 system (Kawakami et al., 2004; Urasaki et al., 2006). Because *Tg[RARE:Venus]* carries 3 x RA response element (RARE, 5′-AGCTTGAAGGGTTCACCGAAAGTTCACTCGCA-3′) (Rossant et al., 1991), human β-globin minimal promoter, *Venus* full-length cDNA and SV40 poly A sequence, we can monitor RA signal activity within zebrafish embryo by observing Venus expression. As it has been reported that 8.5 or 15 ng *raldh2* MO can phenocopy *nls* (Begemann et al., 2001), we injected 8.5 or 15 ng *raldh2* MO into the *Tg[RARE:Venus]* embryos. As expected, Venus expression was strongly reduced, and the *nls* phenotypes (e.g. truncation of hindbrain, small and abnormal shape of somites, and short body) could be seen in the manipulated embryos (supplementary material Fig. S2). Although injection of 1.7 ng *raldh2* MO led to mild defects in hindbrain and trunk, Venus signals were reduced in the manipulated embryos at 10 and 28 hpf (supplementary material Fig. S2). These results therefore suggest that injection of 1.7 ng *raldh2* MO leads to a partial knockdown situation in zebrafish embryos.

For time-lapse imaging, *raldh2* MO (1.7 ng), *deltad* MO (2 ng) or *fgf8a* MO (5 ng) were injected into the yolk of one-cell-stage zebrafish embryos as described previously (Matsui et al., 2011). After time-lapse imaging, embryos were recovered from 1% low melting agarose, left to develop until the indicated time points, and tested whether they show specific phenotypes induced by gene knockdown (supplementary material Fig. S3). Any embryo that did not display the specific gene knockdown phenotypes was excluded from the subsequent analyses.

Rescue experiments

Embryos injected with *raldh2* MO (1.7 ng) were treated with 1 nM RA (Sigma) during at 4-10 or 7-10 hpf. For time-lapse imaging, embryos were immediately mounted in 1% low melting agarose and time-series data were collected. Embryos were then fixed at the indicated time points and used for *in situ* hybridization and skeletal staining.

Statistical analyses

Analysis of variance (ANOVA) method was used for multiple comparisons and significant differences were determined using Scheffe's post-hoc test. Differences in gene expression pattern were analyzed by two-tailed Fisher's exact tests. All statistical analyses were performed using R software. Results were considered significant when $P<0.05$.

Acknowledgements

We are grateful to Shinji Takada for sharing reagents, for helpful discussions and for critical reading of the manuscript. We also thank Ian Smith and Fiqri Dizar Khaidizar for help in preparing the manuscript; Koichi Kawakami, Takashi Akanuma and Jun Koyama for sharing reagents; and Maiko Yokouchi and Hiroko Shigesato for technical assistance.

Competing interests

The authors declare no competing financial interests.

Author contributions

B.R. and R.A. performed the experiments and analyzed data. T. Matta carried out statistical analyses. Y.B. contributed to experimental design. T. Matsui designed and performed the experiments, analyzed data and wrote the manuscript.

Funding

This work was supported by Grants-in-Aid for Scientific Research [23111517 and 24681043 to T.M., 17017027 to Y.B. and T.M.] from the Ministry of Education, Culture, Sports, Science and Technology (MEXT), Japan; and by Mochida Memorial Foundation for Medical and Pharmaceutical Research, Japan.

Supplementary material

Supplementary material available online at
http://dev.biologists.org/lookup/suppl/doi:10.1242/dev.097568/-/DC1

References

Begemann, G., Schilling, T. F., Rauch, G. J., Geisler, R. and Ingham, P. W. (2001). The zebrafish neckless mutation reveals a requirement for raldh2 in mesodermal signals that pattern the hindbrain. *Development* **128**, 3081-3094.

Draper, B. W., Stock, D. W. and Kimmel, C. B. (2003). Zebrafish fgf24 functions with fgf8 to promote posterior mesodermal development. *Development* **130**, 4639-4654.

Dubrulle, J., McGrew, M. J. and Pourquié, O. (2001). FGF signaling controls somite boundary position and regulates segmentation clock control of spatiotemporal Hox gene activation. *Cell* **106**, 219-232.

Duester, G. (2007). Retinoic acid regulation of the somitogenesis clock. *Birth Defects Res. C Embryo Today* **81**, 84-92.

Fior, R., Maxwell, A. A., Ma, T. P., Vezzaro, A., Moens, C. B., Amacher, S. L., Lewis, J. and Saúde, L. (2012). The differentiation and movement of presomitic mesoderm progenitor cells are controlled by Mesogenin 1. *Development* **139**, 4656-4665.

Gajewski, M., Sieger, D., Alt, B., Leve, C., Hans, S., Wolff, C., Rohr, K. B. and Tautz, D. (2003). Anterior and posterior waves of cyclic her1 gene expression are differentially regulated in the presomitic mesoderm of zebrafish. *Development* **130**, 4269-4278.

Garnett, A. T., Han, T. M., Gilchrist, M. J., Smith, J. C., Eisen, M. B., Wardle, F. C. and Amacher, S. L. (2009). Identification of direct T-box target genes in the developing zebrafish mesoderm. *Development* **136**, 749-760.

Geelen, J. A. (1979). Hypervitaminosis A induced teratogenesis. *CRC Crit. Rev. Toxicol.* **6**, 351-375.
Grandel, H. and Brand, M. (2011). Zebrafish limb development is triggered by a retinoic acid signal during gastrulation. *Dev. Dyn.* **240**, 1116-1126.
Hamade, A., Deries, M., Begemann, G., Bally-Cuif, L., Genêt, C., Sabatier, F., Bonnieu, A. and Cousin, X. (2006). Retinoic acid activates myogenesis in vivo through Fgf8 signalling. *Dev. Biol.* **289**, 127-140.
Hanneman, E. and Westerfield, M. (1989). Early expression of acetylcholinesterase activity in functionally distinct neurons of the zebrafish. *J. Comp. Neurol.* **284**, 350-361.
Henry, C. A., Urban, M. K., Dill, K. K., Merlie, J. P., Page, M. F., Kimmel, C. B. and Amacher, S. L. (2002). Two linked hairy/Enhancer of split-related zebrafish genes, her1 and her7, function together to refine alternating somite boundaries. *Development* **129**, 3693-3704.
Holley, S. A. (2006). Anterior-posterior differences in vertebrate segments: specification of trunk and tail somites in the zebrafish blastula. *Genes Dev.* **20**, 1831-1837.
Holley, S. A. (2007). The genetics and embryology of zebrafish metamerism. *Dev. Dyn.* **236**, 1422-1449.
Holley, S. A., Geisler, R. and Nüsslein-Volhard, C. (2000). Control of her1 expression during zebrafish somitogenesis by a delta-dependent oscillator and an independent wave-front activity. *Genes Dev.* **14**, 1678-1690.
Kawakami, K., Takeda, H., Kawakami, N., Kobayashi, M., Matsuda, N. and Mishina, M. (2004). A transposon-mediated gene trap approach identifies developmentally regulated genes in zebrafish. *Dev. Cell* **7**, 133-144.
Kawakami, Y., Raya, A., Raya, R. M., Rodríguez-Esteban, C. and Izpisúa Belmonte, J. C. (2005). Retinoic acid signalling links left-right asymmetric patterning and bilaterally symmetric somitogenesis in the zebrafish embryo. *Nature* **435**, 165-171.
Kawamura, A., Koshida, S., Hijikata, H., Ohbayashi, A., Kondoh, H. and Takada, S. (2005). Groucho-associated transcriptional repressor ripply1 is required for proper transition from the presomitic mesoderm to somites. *Dev. Cell* **9**, 735-744.
Kawamura, A., Koshida, S. and Takada, S. (2008). Activator-to-repressor conversion of T-box transcription factors by the Ripply family of Groucho/TLE-associated mediators. *Mol. Cell. Biol.* **28**, 3236-3244.
Kessel, M. and Gruss, P. (1991). Homeotic transformations of murine vertebrae and concomitant alteration of Hox codes induced by retinoic acid. *Cell* **67**, 89-104.
Kimmel, C. B., Ballard, W. W., Kimmel, S. R., Ullmann, B. and Schilling, T. F. (1995). Stages of embryonic development of the zebrafish. *Dev. Dyn.* **203**, 253-310.
Lee, H. C., Tseng, W. A., Lo, F. Y., Liu, T. M. and Tsai, H. J. (2009). FoxD5 mediates anterior-posterior polarity through upstream modulator Fgf signaling during zebrafish somitogenesis. *Dev. Biol.* **336**, 232-245.
Mara, A., Schroeder, J., Chalouni, C. and Holley, S. A. (2007). Priming, initiation and synchronization of the segmentation clock by deltaD and deltaC. *Nat. Cell Biol.* **9**, 523-530.
Matsui, T., Raya, A., Kawakami, Y., Callol-Massot, C., Capdevila, J., Rodríguez-Esteban, C. and Izpisúa Belmonte, J. C. (2005). Noncanonical Wnt signaling regulates midline convergence of organ primordia during zebrafish development. *Genes Dev.* **19**, 164-175.
Matsui, T., Thitamadee, S., Murata, T., Kakinuma, H., Nabetani, T., Hirabayashi, Y., Hirate, Y., Okamoto, H. and Bessho, Y. (2011). Canopy1, a positive feedback regulator of FGF signaling, controls progenitor cell clustering during Kupffer's vesicle organogenesis. *Proc. Natl. Acad. Sci. USA* **108**, 9881-9886.
Morin-Kensicki, E. M., Melancon, E. and Eisen, J. S. (2002). Segmental relationship between somites and vertebral column in zebrafish. *Development* **129**, 3851-3860.
Niederreither, K. and Dollé, P. (2008). Retinoic acid in development: towards an integrated view. *Nat. Rev. Genet.* **9**, 541-553.
Nikaido, M., Kawakami, A., Sawada, A., Furutani-Seiki, M., Takeda, H. and Araki, K. (2002). Tbx24, encoding a T-box protein, is mutated in the zebrafish somite-segmentation mutant fused somites. *Nat. Genet.* **31**, 195-199.
Pourquié, O. (2001). Vertebrate somitogenesis. *Annu. Rev. Cell Dev. Biol.* **17**, 311-350.
Resende, T. P., Ferreira, M., Teillet, M. A., Tavares, A. T., Andrade, R. P. and Palmeirim, I. (2010). Sonic hedgehog in temporal control of somite formation. *Proc. Natl. Acad. Sci. USA* **107**, 12907-12912.
Rossant, J., Zirngibl, R., Cado, D., Shago, M. and Giguère, V. (1991). Expression of a retinoic acid response element-hsplacZ transgene defines specific domains of transcriptional activity during mouse embryogenesis. *Genes Dev.* **5**, 1333-1344.
Sawada, A., Shinya, M., Jiang, Y. J., Kawakami, A., Kuroiwa, A. and Takeda, H. (2001). Fgf/MAPK signalling is a crucial positional cue in somite boundary formation. *Development* **128**, 4873-4880.
Schröter, C., Herrgen, L., Cardona, A., Brouhard, G. J., Feldman, B. and Oates, A. C. (2008). Dynamics of zebrafish somitogenesis. *Dev. Dyn.* **237**, 545-553.
Schubert, M., Holland, L. Z., Stokes, M. D. and Holland, N. D. (2001). Three amphioxus Wnt genes (AmphiWnt3, AmphiWnt5, and AmphiWnt6) associated with the tail bud: the evolution of somitogenesis in chordates. *Dev. Biol.* **240**, 262-273.
Tam, P. P. (1981). The control of somitogenesis in mouse embryos. *J. Embryol. Exp. Morphol.* **65 Suppl.**, S103-S128.
Urasaki, A., Morvan, G. and Kawakami, K. (2006). Functional dissection of the Tol2 transposable element identified the minimal cis-sequence and a highly repetitive sequence in the subterminal region essential for transposition. *Genetics* **174**, 639-649.
Wright, G. J., Giudicelli, F., Soza-Ried, C., Hanisch, A., Ariza-McNaughton, L. and Lewis, J. (2011). DeltaC and DeltaD interact as Notch ligands in the zebrafish segmentation clock. *Development* **138**, 2947-2956.
Yamamoto, A., Amacher, S. L., Kim, S. H., Geissert, D., Kimmel, C. B. and De Robertis, E. M. (1998). Zebrafish paraxial protocadherin is a downstream target of spadetail involved in morphogenesis of gastrula mesoderm. *Development* **125**, 3389-3397.

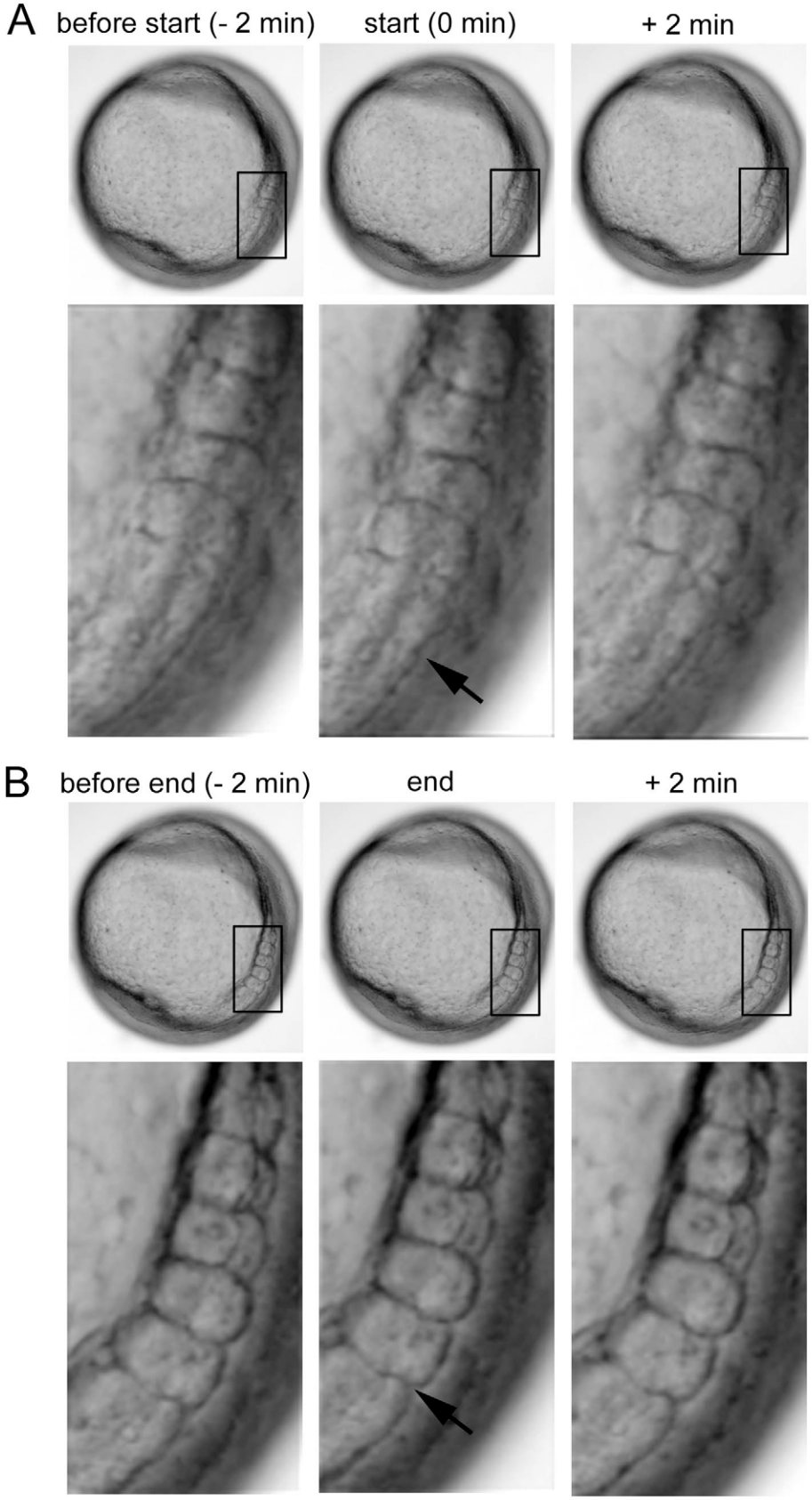

Figure S1 Start and end of somite segmentation. (A) Representative images of segmentation start. Lateral view, dorsal to the right. Lower panel: higher-magnification views of boxed areas. A furrow (arrow) appeared at the dorsal limit of the presomitic mesoderm at 0 min. Two min later, the furrow became clearer. (B) Representative images of segmentation end. Lower panel: higher-magnification views of boxed areas. The somite boundary (arrow) became clearer, and the somite and presomitic mesoderm were completely separated. Panels are frames of Movie 1.

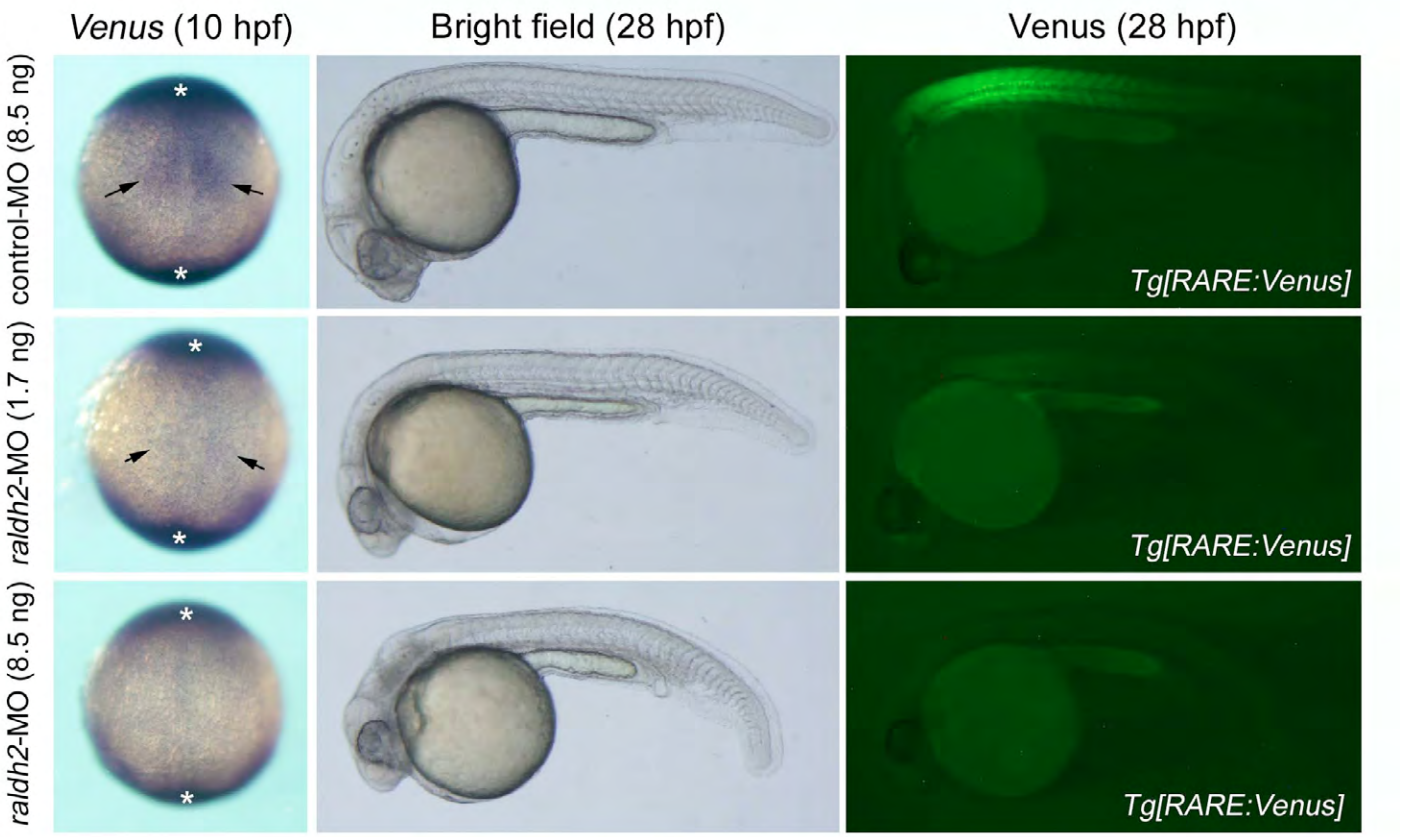

Figure S2 Knockdown efficiency of *raldh2* evaluated by using *Tg[RARE:Venus]* embryos. Left panel: Representative images of Venus expression in 10 hpf embryos injected with 8.5 ng control-MO (n = 42), 1.7 ng *raldh2*-MO (n = 34) or 8.5 ng *raldh2*-MO (n = 38). Dorsal view, anterior to the top. *in situ* signal marked by asterisk was considered as a background signal because similar signal could be detected in wildtype embryos and because *raldh2* is not expressed in these regions. Center and right panel: Representative images of Venus expression in 28 hpf embryos injected with 8.5 ng control-MO (n = 57), 1.7 ng *raldh2*-MO (n = 34) or 8.5 ng *raldh2*-MO (n = 41). Lateral view, anterior to the left. RA signal activity (Venus signals) could be seen at a part of paraxial mesoderm (arrow) in control embryos at 10 hpf, and at anterior somites and eyes in control embryos at 28 hpf (upper panels). The activity was detected weakly in embryos injected with 1.7 ng *raldh2*-MO (middle panels), but not in embryos injected with 8.5 ng *raldh2*-MO (lower panels).

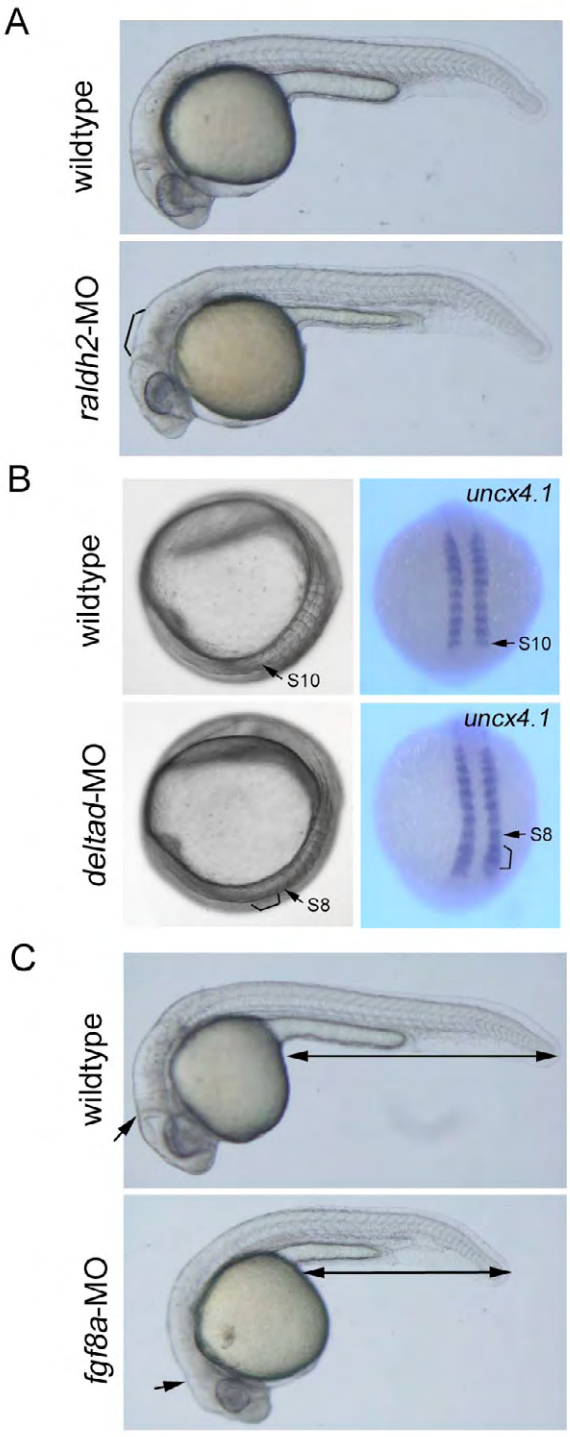

Figure S3 Evaluation of MO activity after time-lapse imaging. (A) *raldh2* morphants. Embryos (24 – 30 hpf) showing defects in hindbrain (bracket) and trunk somites were selected and used to further analyses. (B) *deltad* morphants. Embryos (14 hpf) which phenocopy *after eight* (*deltad* mutants) were selected. In these embryos, segmentation defects could be seen around S8 – 10 (bracket). (C) *fgf8a* morphants. Embryos (24 – 30 hpf) that phenocopy *ace* (*fgf8a* mutants) were selected. Defects in midbrain-hindbrain boundary (arrow) and tail elongation (double arrow) could be seen in phenocopied embryos.

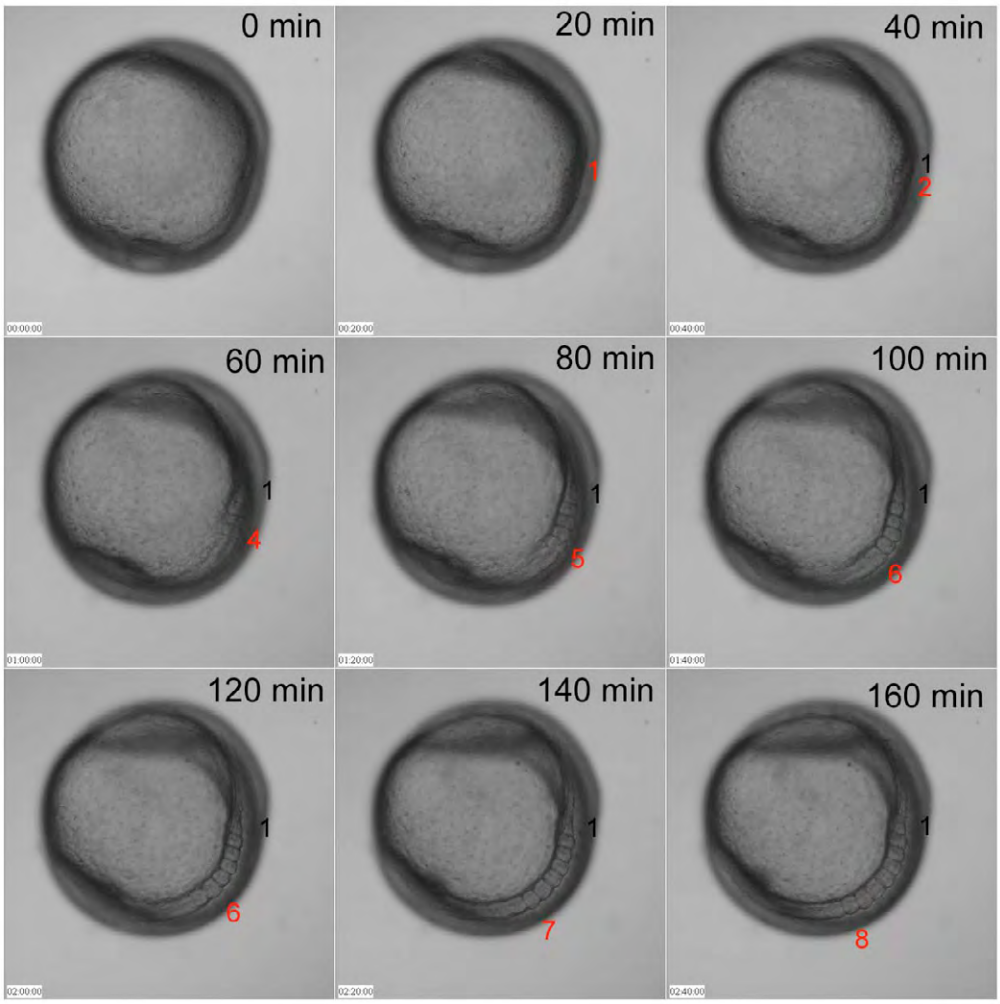

Figure S4 A difference between anterior and posterior somitogenesis. Time-lapse images every 20 min are displayed. The first somite (numbered 1) and the newest somite at each time point (red) are indicated. Panels are frames of Movie 1.

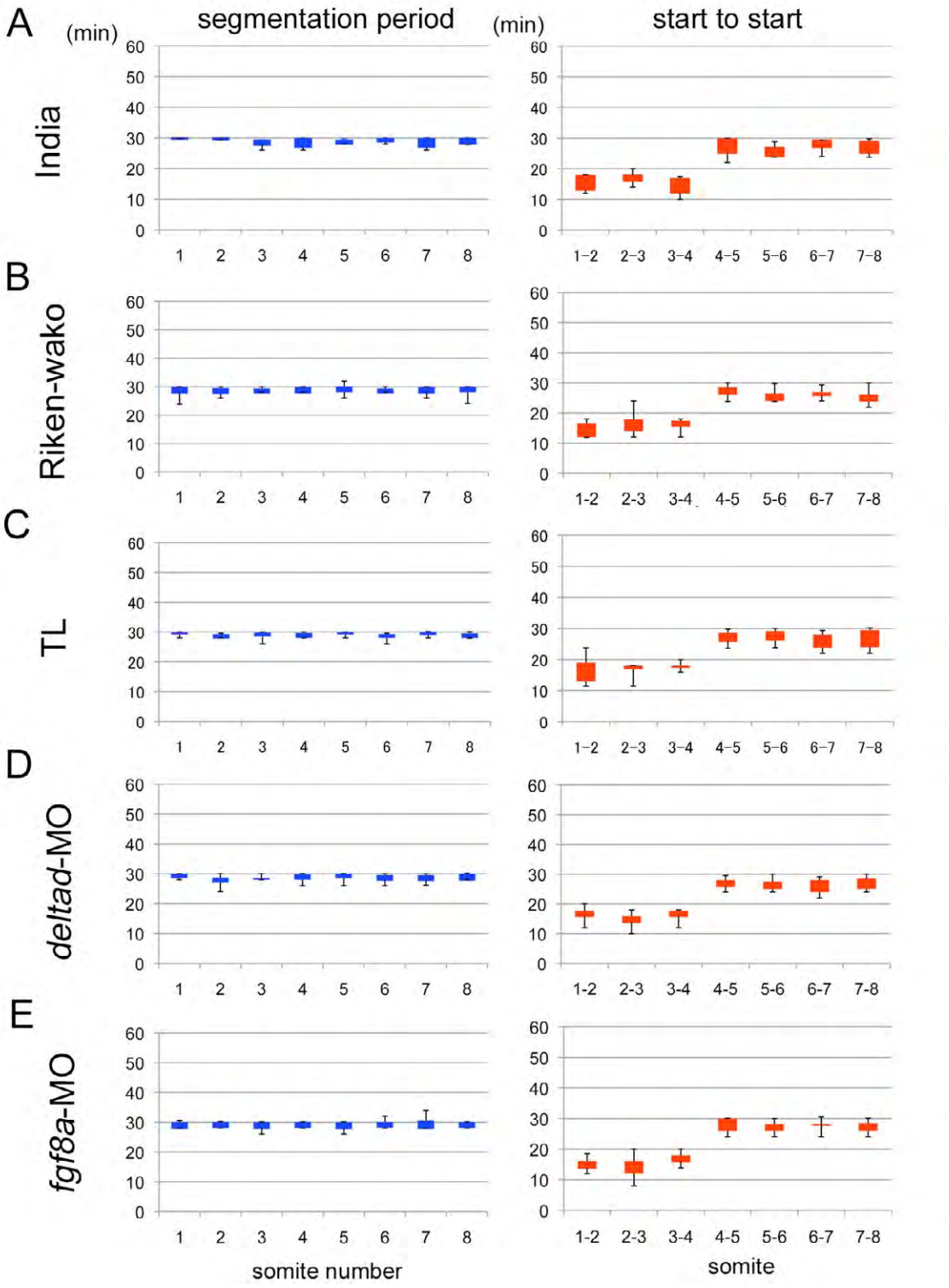

Figure S5 The AP difference occurs in several wildtype strains and in *deltad* and *fgf8a* morphants. Left panel: segmentation period; right panel: start to start. (A) India (n = 8). (B) Riken-wako (n = 8). (C) TL (n = 7). (D) *deltad* morphants (n = 7). (E) *fgf8a* morphants (n = 9).

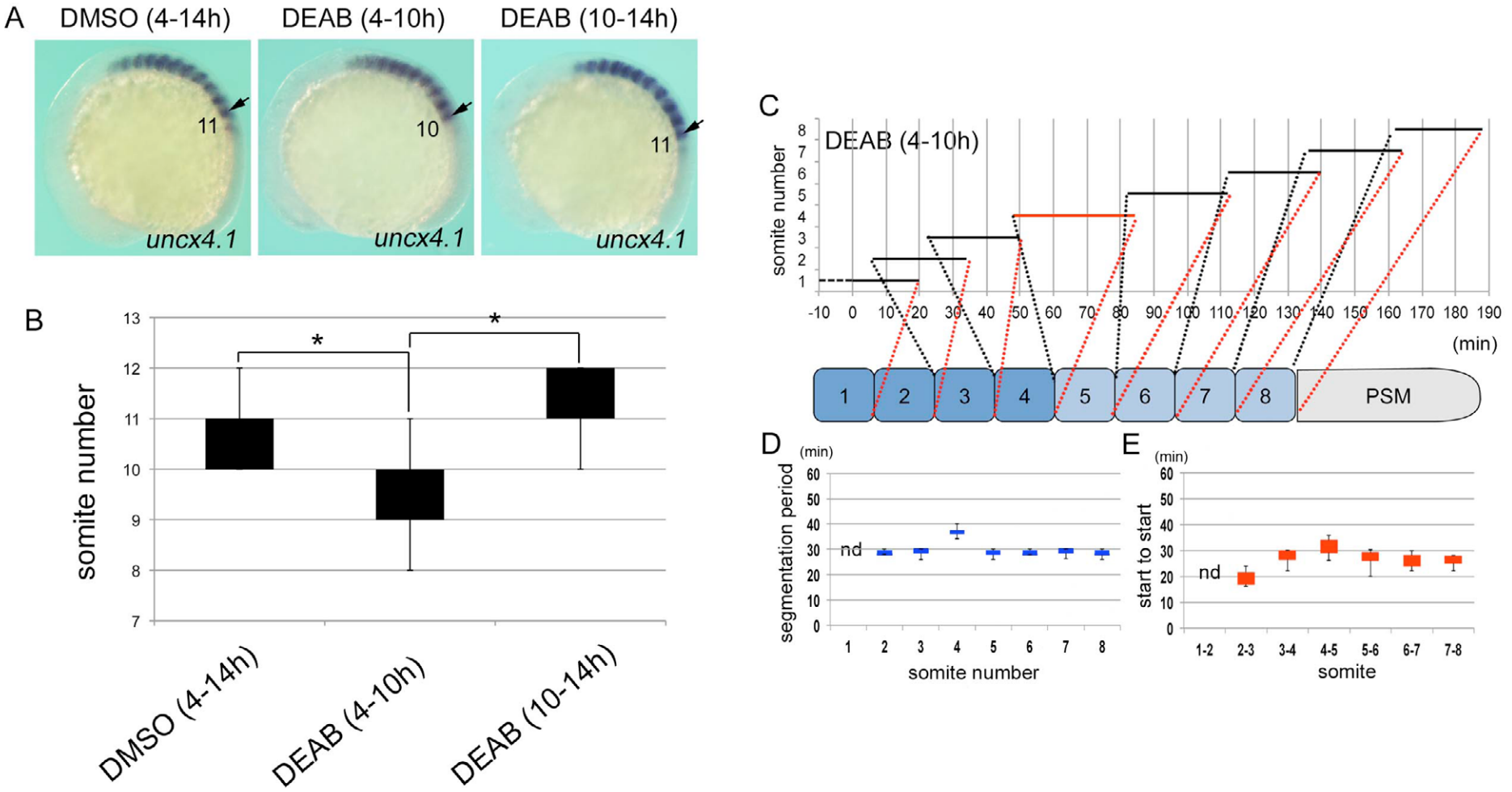

Figure S6 Inhibition of RA synthesis during gastrulation results in loss of a somite. (A) Representative images of *uncx4.1* expression in embryos treated with DMSO (4 – 14 hpf) (left), DEAB (4 – 10 hpf) (center) or DEAB (10 – 14 hpf) (right). Lateral view, anterior to the left. Arrows marked the position at SI. (B) Box and whisker plots of somite number in embryos treated with DMSO (4 – 14 hpf) (n = 34), DEAB (4 – 10 hpf) (n = 29) or DEAB (10 – 14 hpf) (n = 25). Statistically significant difference (asterisk, $P < 0.05$) could be seen in DMSO versus DEAB (4 – 10 hpf), and DEAB (4 – 10 hpf) versus DEAB (10 – 14 hpf). (C) Time-lapse data for somitogenesis in an embryo treated with DEAB (4 – 10 hpf) (see Movie 4, 4-1). (D, E) Box and whisker plots of segmentation period (D) or start to start (E) for embryos treated with DEAB during 4 – 10 hpf (n = 8). Results from statistical analyses are shown in Table S1 – 4.

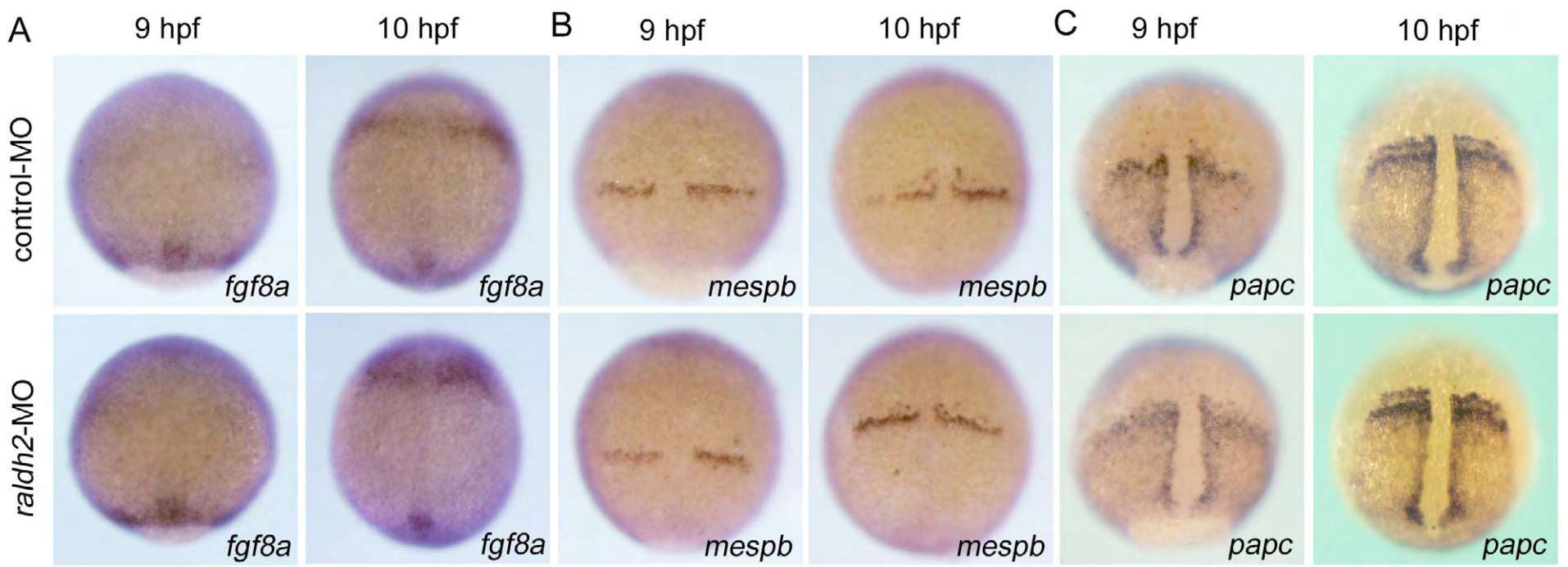

Figure S7 *raldh2* knockdown does not affect expression of *fgf8a*, *mespb* or *papc*. Expression of *fgf8a* (A), *mespb* (B) or *papc* (C) in control (upper) or *raldh2* morphants (lower) at 9 (left) or 10 hpf (right).

Movie 1A. This movie shows the lateral view of a wildtype embryo. The time-lapse covers the period of 10 – 13 hpf.

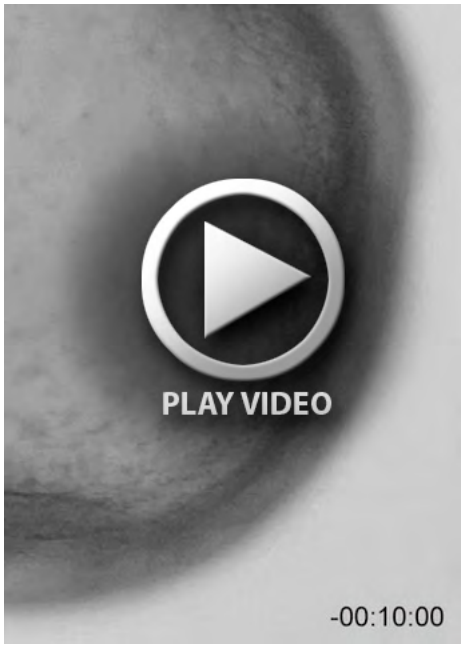

Movie 1B. Higher-magnification views of somite areas in Movie 1A. Black and red arrows indicate start and end of morphological segmentation.

Movie 2. This movie shows the lateral view of a wildtype embryo. The time-lapse covers the period of 13 – 16 hpf.

Movie 3A. This movie shows the lateral view of a wildtype embryo injected with *raldh2*-MO (a *raldh2* morphant). The time-lapse covers the period of 10 – 13 hpf.

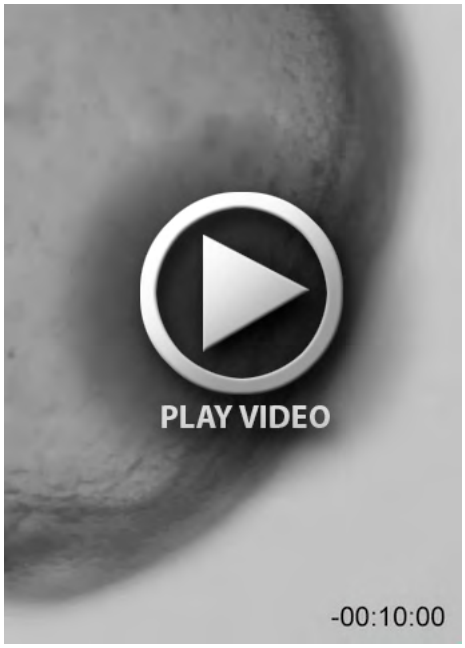

Movie 3B. Higher-magnification views of somite areas in Movie 3A. Black and red arrows indicate start and end of morphological segmentation.

Movie 4A. This movie shows the lateral view of a wildtype embryo treated with DEAB (4 – 10 hpf). The time-lapse covers the period of 10 – 13 hpf.

Movie 4B. Higher-magnification views of somite areas in Movie 4A. Black and red arrows indicate start and end of morphological segmentation.

Movie 5A. This movie shows the lateral view of a *raldh2* morphant treated with RA (4 – 10 hpf). The time-lapse covers the period of 10 – 13 hpf.

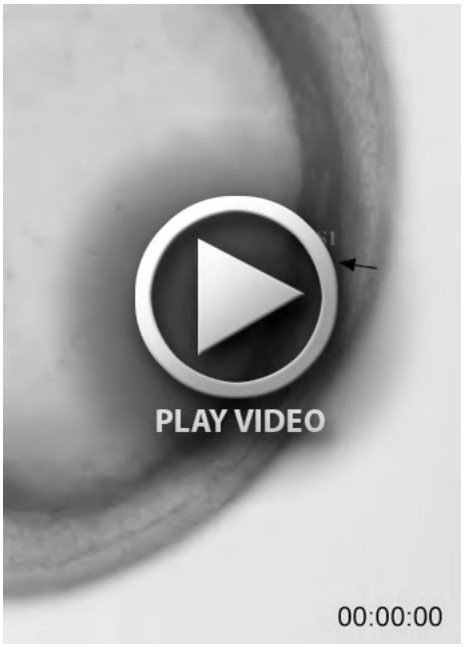

Movie 5B. Higher-magnification views of somite areas in Movie 5A. Black and red arrows indicate start and end of morphological segmentation.

Table S1.

Download Table S1

Table S2.

Download Table S2

Table S3.

Download Table S3

Table S4.

Download Table S4

Table S5.

Download Table S5

Table S6.

Download Table S6

Table S7.

Download Table S7

Table S8.

Download Table S8